

1 Citation: **Hirt C.**, M. Kuhn, S.J. Claessens, R. Pail, K. Seitz, T. Gruber (2014), Study of the
2 Earth's short-scale gravity field using the ERTM2160 gravity model, Computers &
3 Geosciences, 73, 71-80, doi: 10.1016/j.cageo.2014.09.00.

4 **Study of the Earth's short-scale gravity field using the** 5 **ERTM2160 gravity model**

6 **Christian Hirt**

8 Western Australian Centre for Geodesy & The Institute for Geoscience Research,
9 Curtin University, Perth, Australia

10 Currently at: Institute for Astronomical and Physical Geodesy, Technische Universität
11 München, Germany

12 Email: c.hirt@curtin.edu.au

13

14 **Michael Kuhn**

15 Western Australian Centre for Geodesy & The Institute for Geoscience Research,
16 Curtin University, Perth, Australia

17 Email: m.kuhn@curtin.edu.au

18

19 **Sten Claessens**

20 Western Australian Centre for Geodesy & The Institute for Geoscience Research,
21 Curtin University, Perth, Australia

22 Email: s.claessens@curtin.edu.au

23

24 **Roland Pail**

25 Institute for Astronomical and Physical Geodesy, Technische Universität München,
26 Germany

27 Email: pail@bv.tum.de

28

29 **Kurt Seitz**

30 Geodetic Institute, Karlsruhe Institute of Technology (KIT), Karlsruhe,
31 Germany

32 Email: kurt.seitz@kit.edu

33

34 **Thomas Gruber**

35 Institute for Astronomical and Physical Geodesy, Technische Universität München,
36 Germany

37 Email: thomas.gruber@tum.de

38

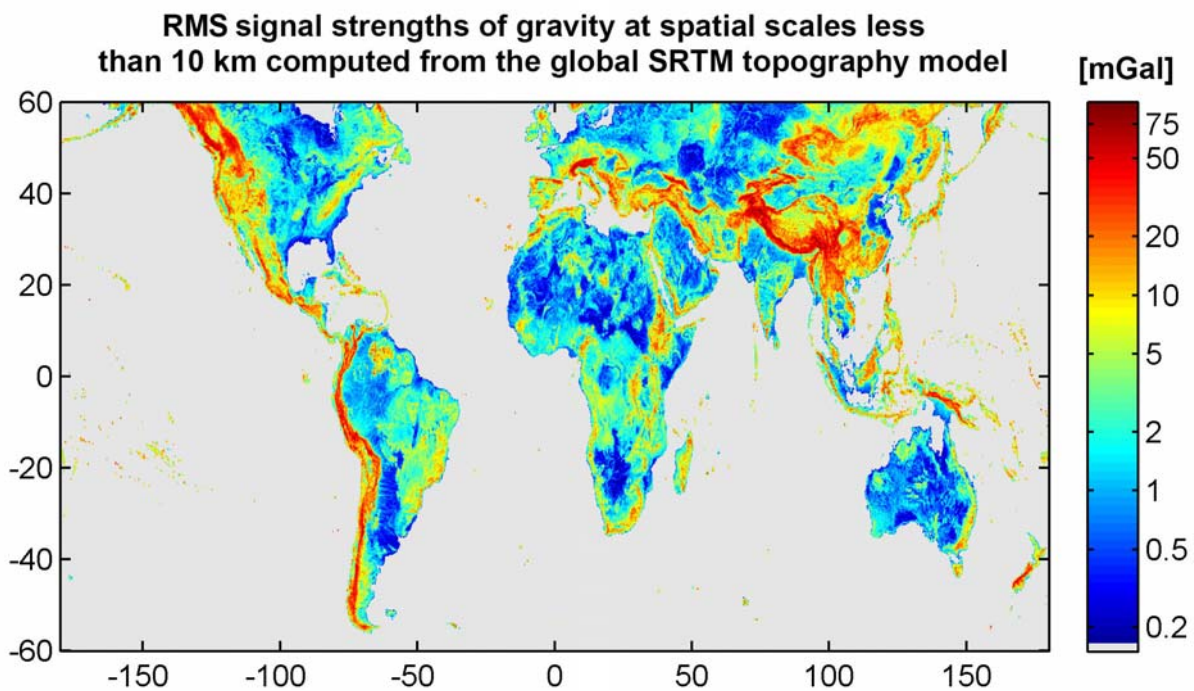
39 **Abstract**

40 This paper describes the computation and analysis of the Earth's short-scale gravity field
41 through high-resolution gravity forward modelling using the Shuttle Radar Topography
42 Mission (SRTM) global topography model. We use the established residual terrain modelling
43 technique along with advanced computational resources and massive parallelisation to
44 convert the high-pass filtered SRTM topography – complemented with bathymetric
45 information in coastal zones – to implied short-scale gravity effects. The result is the
46 ERTM2160 model (Earth Residual Terrain modelled-gravity field with the spatial scales
47 equivalent to spherical-harmonic coefficients up to degree 2160 removed). ERTM2160, used
48 successfully for the construction of the GGMplus gravity maps, approximates the short-scale

49 (i.e., ~10 km down to ~250 m) gravity field in terms of gravity disturbances, quasi/geoid
50 heights and vertical deflections at ~3 billion gridded points within ± 60 latitude. ERTM2160
51 reaches maximum values for the quasi/geoid height of ~30 cm, gravity disturbance in excess
52 of 100 mGal, and vertical deflections of ~30 arc-seconds over the Himalaya mountains.
53 Analysis of the ERTM2160 field as a function of terrain roughness shows in good
54 approximation a linear relationship between terrain roughness and gravity effects, with values
55 of ~1.7 cm (quasi/geoid heights), ~11 mGal (gravity disturbances) and 1.5 arc-seconds
56 (vertical deflections) signal strength per 100 m standard deviation of the terrain. These
57 statistics can be used to assess the magnitude of omitted gravity signals over various types of
58 terrain when using degree-2160 gravity models such as EGM2008. Applications for
59 ERTM2160 are outlined including its use in gravity smoothing procedures, augmentation of
60 EGM2008, fill-in for future ultra-high resolution gravity models in spherical harmonics, or
61 calculation of localized or global power spectra of Earth's short-scale gravity field.
62 ERTM2160 is freely available via <http://ddfe.curtin.edu.au/gravitymodels/ERTM2160>.

63
64
65

Graphical Abstract



Highlights

70

- 71 • Residual gravity model ERTM2160 computed from the SRTM topography at 250 m
72 resolution
- 73 • Supercomputing resources used for forward gravity modelling at ~3 billion points
- 74 • Global short-scale RMS signal magnitudes are 1.6 cm for geoid, 11 mGal for gravity
- 75 • Linear relation between terrain roughness and RMS gravity signal magnitudes found

76

Key words

77

78

79

Gravity field, forward-modelling, gravity, quasi/geoid, vertical deflection, supercomputing

80

81 1 Introduction

82

83 Forward-modelling of the gravity field from topographic mass models is central to physical
84 geodesy and potential field geophysics (e.g., Forsberg, 1984; Jacoby and Smilde, 2009). All
85 gravity forward modelling techniques are based on the evaluation of Newton's integral (Kuhn
86 and Seitz, 2005) which can be done either in the spectral domain (Rummel et al., 1988;
87 Balmino et al., 2012), or in the space domain (Forsberg, 1984; Nagy et al., 2000). For gravity
88 forward modelling in the space domain, the topographic masses are usually represented
89 through gridded digital elevation models decomposing the terrain into discrete geometrical
90 mass-bodies (i.e., point masses, prisms or tesseroids), cf. Heck and Seitz (2007). The
91 practical evaluation of Newton's integral at a single computation point P involves numerical
92 integration (summation) of gravity effects generated by each geometrical mass-body to some
93 distance around P (Tziavos and Sideris, 2013) when evaluating short-scale gravity effects and
94 global numerical integration when evaluating full-scale gravity effects (e.g. Kuhn et al.,
95 2009).

96

97 Until recently, one of the limiting factors for the application of space domain techniques in
98 ultra-high resolution forward modelling on regional to global scales was their enormous
99 computational demand. This is due to the fact that Newton's integral has to be evaluated
100 separately for each computation point without drawing information from other already
101 evaluated gravity effects. Therefore, the required number of operations increases linearly
102 with the number of computation points, which is why ultra-high resolution (i.e., spatial
103 density of P commensurate to the elevation data resolution, say ~ 100 - 200 m) gravity forward
104 modelling on a global scale is a computationally demanding task. However, this drawback
105 can also be used as advantage when employing parallel computation techniques as the
106 gravitational effect at each computation point can be obtained independently of all other
107 points. This advantage has been exploited in this study through the use of advanced
108 computational resources along with parallelization of the computations.

109

110 This study focuses on (i) gravity forward-modelling of the Earth's short-scale gravity field
111 from the high-resolution SRTM topography (augmented with bathymetry in coastal zones) in
112 the space domain, and (ii) analysis of gravity signal magnitudes with spatially varying
113 statistics. The term "short-scale" is defined here as spatial scales of ~ 10 km (or beyond
114 spherical harmonic degree 2160) down to ~ 250 m. The target area for our ultra-high
115 resolution gravity forward-modelling are all continents between $\pm 60^\circ$ geodetic latitude as
116 represented through the Shuttle Radar Topography Mission (SRTM) global elevation model,
117 including adjoining coastal zones, Earth's major lakes and numerous islands. Using a dense
118 grid spacing of 7.2 arc-sec, there are more than 3 billion computation points in our near-
119 global target area, which necessitates the use of advanced computational resources and
120 parallelization of the forward-modelling task. The main result of the gravity forward
121 modelling is a model that describes Earth's short-scale gravity field (over our target area) in
122 terms of quasi/geoid heights, gravity disturbances and vertical deflections: ERTM2160 (Earth
123 Residual Terrain Modelled - gravity field with the 2160 indicating that spatial scales up to
124 spherical-harmonic degree and order 2160 were removed).

125

126 ERTM2160 was created in the context of the GGMplus (Global Gravity Maps plus) initiative
127 (Hirt et al., 2013) to deliver the short-scale constituents for the GGMplus gravity maps
128 (<http://geodesy.curtin.edu.au/research/GGMplus>). While Hirt et al. (2013) give a general
129 description of the gravity forward modelling and the combination of forward-modelled
130 gravity with observed gravity data used to construct GGMplus, we here provide a full

131 account of the conversion of the global SRTM topography to short-scale ERTM2160 gravity
132 effects (Sect. 2), and present an entirely new analysis of their statistical characteristics (Sect
133 3). In order to provide a complete description of the methods deployed, the methods and data
134 summary (Sect. 2) has deliberately some overlap with previously reported research (Hirt et
135 al., 2013; Hirt, 2013).

136

137 Regarding the gravity forward-modelling applied with ultra-high resolution on a near-global
138 scale, new research presented in this study includes (i) the role of accurate high-pass filtering
139 for short-scale gravity forward modelling, (ii) the treatment of major lakes in the forward
140 modelling and (iii) identification and removal of low-quality and bad-data areas in the
141 topography models (data cleaning) cf. Sect 2. The main focus is placed in this paper on
142 studying the characteristics of the ERTM2160 short-scale gravity field. New results presented
143 include (i) magnitude statistics of gravity anomalies, geoid heights and vertical deflections,
144 (ii) a first comparison with estimates from degree-variances models, and (iii) the
145 investigation of the functional relationship among gravity signal strengths and terrain
146 roughness (Sect. 3). We further summarize application examples (Sect. 4) and outline
147 limitations for ERTM2160 (Sect. 5), before making some concluding remarks (Sect. 6).

148

149 Apart from Hirt et al. (2013), results from ultra-high resolution (say few 100 m) gravity
150 forward-modelling on a near-global scale were not yet reported in the literature. Thus far,
151 gravity forward-modelling is either limited in spatial resolution (say 1-2 arc-min, or ~2-4 km)
152 when done globally, e.g., Gruber et al. (2013); Balmino et al. (2012); Bonvalot et al. (2012),
153 or limited to regional areas when done with ultra-high resolution (say around 250 m), e.g.,
154 Kuhn et al. (2009). It is only through the computation of ERTM2160 that the study of the
155 short scale gravity field characteristics has become possible at a near-global scale and with
156 ultra-high resolution.

157

158 **2. Data and methods**

159

160 **2.1 Data sets and combination**

161 As high-resolution representations of the topographic masses over land, we selected the ~250
162 m (7.5 arc-sec) resolution SRTM V4.1 topography model provided by Jarvis et al. (2008).
163 This data set is based on the second (research-grade) release of the SRTM mapping mission
164 (Farr et al. 2007), with improved interpolation methods often based on auxiliary data sets
165 used for filling of no-data areas ('holes'), as described by Reuter et al. (2007). The resolution
166 of the V4.1 250 m version, derived by Jarvis et al. (2008) from the 90 m SRTM basis
167 resolution, is commensurate with the ERTM2160 target resolution of 7.2 arc-sec. The SRTM
168 V4.1 topography model is available within the $\pm 60^\circ$ latitude SRTM coverage, and
169 incorporates coastline information through the SRTM water body data set. The SRTM
170 elevation model is referred to the EGM96 geoid model (resolution of degree and order 360).

171 In order to avoid 'edge effects' of the SRTM-based forward-modelling along coast lines and
172 at $\pm 60^\circ$ latitude, we included – outside the V4.1 coverage – bathymetric depth information
173 as available through the 30 arc-sec resolution V7 SRTM30_PLUS topography/bathymetry
174 model (Becker et al. 2009). The bathymetric component of the SRTM30_PLUS data set is
175 based on altimetry and – where available – depth soundings (Becker et al., 2009).
176 SRTM30_PLUS also contains bathymetric information for Earth's major lakes (Great Lakes,
177 Caspian Sea, Baikal) which is taken into account in ERTM2160 (Sect. 2.2). According to
178 Becker et al. (2009) SRTM30_PLUS provides GTOPO30 data (USGS 1996) in high northern

179 latitudes, which is a relevant data source for forward-modelling at ERTM2160 computation
 180 points near or at 60° latitude.

181
 182 Following a case study by Hirt (2013) both data sets are combined at 7.5 arc-sec resolution
 183 whereby SRTM30_PLUS data is used everywhere outside the V4.1 data coverage. This
 184 ensures a mostly smooth transition from land to oceans and land to interior lakes, as well as at
 185 the northern and southern extent of the SRTM coverage. SRTM V4.1 and its combination
 186 with SRTM30_PLUS have proven suitable for short-scale gravity forward-modelling over
 187 local and regionally limited land areas (e.g., Hirt, 2012) as well as along some coastal zones
 188 (Hirt, 2013). Notwithstanding it is important to note that at a global scale both data sets are
 189 not free of errors and artefacts, necessitating some data cleaning as described in Sect 2.5.

190

191 **2.2 Treatment of water bodies**

192

193 We make use of the concept of rock-equivalent topography (RET; Rummel et al. 1988),
 194 allowing convenient treatment of topographic and water masses in forward-modelling with a
 195 single constant mass-density. In the RET concept, the lake and ocean water masses are
 196 condensed ('compressed') into layers of rock. With the standard rock mass-density $\rho = 2670$
 197 kg m^{-3} , and ocean water mass-density $\rho_o = 1030 \text{ kg m}^{-3}$, RET-heights $H_{RET}^{(sea)}$ are obtained
 198 over the oceans

$$199 \quad H_{RET}^{(sea)} = H_{BED} \left(1 - \frac{\rho_o}{\rho} \right), \quad (1)$$

200 whereby H_{BED} (<0) is the bathymetric depth with respect to mean sea level (MSL) from
 201 SRTM30_PLUS. For inland water bodies, RET-heights $H_{RET}^{(lakes)}$ are calculated from

202

$$203 \quad H_{RET}^{(lakes)} = H_{BED} + \frac{\rho_L}{\rho} (H_{SUR} - H_{BED}), \quad (2)$$

204 where $\rho_L = 1000 \text{ kg m}^{-3}$ is the lake water mass-density, H_{SUR} is the height of the water body
 205 above MSL (as implied by the SRTM V4.1 model), and H_{BED} is the height of the lake
 206 bottom, taken from SRTM30_PLUS ($H_{SUR} - H_{BED}$ is the water column height). Table 1 lists
 207 the water bodies considered in the present work at 30 arc-sec resolution. We acknowledge
 208 recent work by Balmino et al. (2012) who have forward-modelled gravity effects implied by
 209 the water-masses of several great lakes at 1 arc-min resolution, and Grombein et al. (2014) at
 210 5 arc-min resolution.

211

212

213 **Table 1** Water bodies modelled in ERTM2160, and surface heights (extracted from SRTM V4.1)

Water body	Surface height H_{SUR} [m]
Oceans	0
Caspian Sea	-29
Lake Baikal	+449
Lake Superior	+179
Lake Michigan and Huron	+175
Lake Erie	+172
Lake Ontario	+73

214

215

216 **2.3 High-pass filtering**

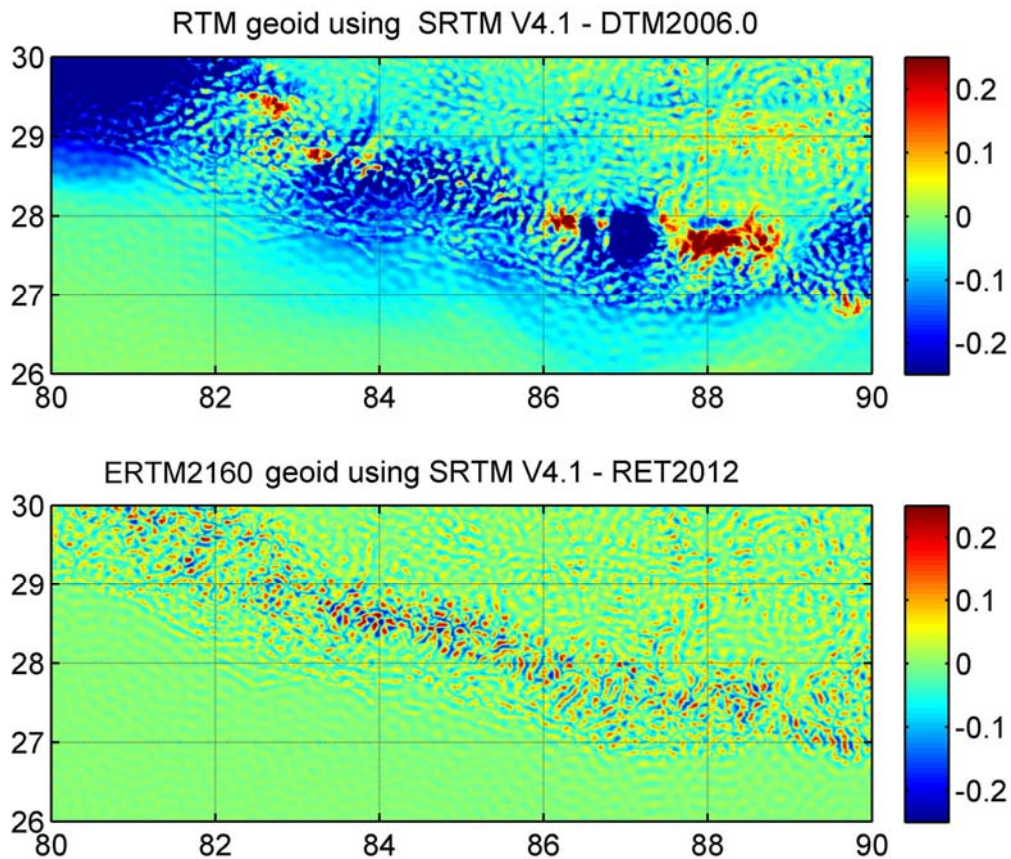
217

218 In short-scale gravity forward-modelling based on the well-established residual terrain
 219 modelling (RTM) technique (Forsberg and Tscherning, 1981; Forsberg, 1984), accurate high-
 220 pass filtering of the elevation data is crucial. Subtraction of a long-wavelength spherical
 221 harmonic reference surface is suitable to extract the short-scale information from elevation
 222 models, particularly when gravity forward-modelling is used for augmentation of GGMs
 223 beyond their nominal resolution (e.g., Forsberg, 1984; Hirt, 2010). For the generation of the
 224 ERTM2160 short-scale gravity model, a spherical harmonic reference surface (denoted with
 225 RET2012 in the sequel) has been developed that is rigorously consistent to the input
 226 topography (SRTM V4.1 over (dry) land and rock-equivalent heights from SRTM30_PLUS
 227 over the oceans and lakes) everywhere over our target area with the procedure described in
 228 Hirt (2013). The fully-normalized RET2012 spherical harmonic coefficients (SHCs)
 229 $\overline{HC}_{nm}, \overline{HS}_{nm}$ are evaluated here to degree and order 2160

230
$$H = \sum_{n=0}^{2160} \sum_{m=0}^n (\overline{HC}_{nm} \cos m\lambda + \overline{HS}_{nm} \sin m\lambda) \overline{P}_{nm}(\sin \varphi) \quad (3)$$

231 with φ and λ are the geocentric latitude and longitude, and $\overline{P}_{nm}(\sin \varphi)$ are the fully-
 232 normalized associated Legendre functions. Subtracting the synthesized heights H from the
 233 high-resolution RET-topography provides the high-pass filtered SRTM data for the
 234 ERTM2160 forward-modelling.

235



236

237 **Fig. 1** Top: RTM geoid effects based on SRTMV4.1 and DTM2006.0 as long-wavelength reference
 238 surface over a 4°x10° test area in the Himalayas, Bottom: ERTM2160 quasi/geoid calculated based on
 239 SRTM V4.1 and RET2012 as rigorously consistent long-wavelength reference surface, units in m. All
 240 maps are coordinated in terms of geodetic latitudes and longitudes, unit degree.

241

242

243 We have tested the spherical harmonic expansion of the DTM2006.0 data created by the
244 EGM2008 development team (Pavlis et al., 2007; 2012) as alternative reference surface for
245 high-pass filtering of the SRTM V4.1 topography and SRTM30_PLUS V7 rock-equivalent
246 bathymetry. Fig. 1 compares forward-modelled quasi/geoid effects over the Himalaya using
247 synthesized heights from DTM2006 (top) and RET2012 (bottom) for high-pass filtering of
248 the SRTM V4.1 topography. From Fig. 1, the combination SRTM V4.1 minus DTM2006.0
249 produces regional-scale offsets with amplitudes at the dm-level over the Himalayas, while
250 SRTMV4.1 minus RET2012 does not show such effects.

251

252 Fig. 1 shows indirectly that SRTM V4.1 and the SRTM release used for the DTM2006.0 data
253 base (Pavlis et al., 2007) are not compatible, with likely differences in the hole-filling
254 procedures used. A similar behaviour as displayed in Fig. 1 is visible over other parts of the
255 Himalayas and parts of the Andes, suggesting inconsistencies between the elevation data
256 bases. While DTM2006.0 was used successfully in earlier studies on forward-modelling over
257 European test areas (e.g., Hirt et al., 2010; Hirt, 2012), DTM2006.0 cannot be used along
258 with SRTM V4.1 over some rugged land areas for accurate high-pass filtering and short-scale
259 forward-modelling. Further inconsistencies would occur over marine areas, even if
260 DTM2006.0 depths were made rock-equivalent. This is because the bathymetry grids used for
261 creating DTM2006.0 and RET2012 are different as well. In the remainder of this paper we
262 therefore only use RET2012 as rigorously consistent long-wavelength reference for our
263 topography/bathymetry-combined RET input grid.

264

265 **2.4 Forward-modelling and use of supercomputing facilities**

266

267 The short-scale gravity forward-modelling, i.e., the conversion of the high-pass filtered and
268 rock-equivalent SRTM topography to gravitational effects, relies on the RTM technique. The
269 gravity field functionals computed are (i) quasi/geoid heights, (ii) gravity disturbances, (iii)
270 North-South vertical deflections, and (iv) East-West vertical deflections. Using regularly-
271 spaced 7.2 arc-sec grids of computation points P over all continents, and adjoining marine
272 areas within $\pm 60^\circ$ latitude, the numerical integration needs to be carried out at more than 3
273 billion locations.

274

275 We used software based on Forsberg's TC-program that deploys mass-prisms (e.g. Nagy et
276 al., 2000) in the ~ 5 km near-zone, point-masses and McMillan expansions in the far-zone
277 (Forsberg, 1984). Different to the original TC-approach, we do not distinguish between
278 different mass-densities over land and oceans in the forward-modelling. Instead we use the
279 high-pass filtered SRTM land topography (over dry land) and SRTM30_PLUS rock-
280 equivalent topography (over water bodies) as input data (Sect. 2.3), along with a single
281 uniform mass-density of 2670 kg m^{-3} (Hirt, 2013). In the RTM technique, the forward-
282 modelling needs to be carried out only to some distance around P (Forsberg, 1984). When
283 high-pass filtering the topography with a degree-2160 spherical harmonic reference surface
284 (equivalent to ~ 10 km), it is sufficient for all gravity functionals computed to take into
285 account mass-effects only within ~ 200 km radius (Hirt et al., 2010). Beyond this radius,
286 mass-prism effects largely cancel out because of the oscillating nature of RTM elevations
287 (see also Forsberg and Tscherning, 1981).

288

289 We divided the gravity forward-modelling task in $1^\circ \times 1^\circ$ regions over land and sea, which
290 can be processed in parallel, i.e., independent of each other. This straightforward and efficient
291 approach of parallelization is taken here because computation points P can be computed

292 without dependencies from each other. The resolution of the input topography is down-
293 sampled from 7.5 arc-sec to 30 arc-sec outside ~ 100 km radius around P (using a 4 x 4 box
294 means), reducing the number of mass-elements and thus the required computation time (two-
295 grid approach, cf. Forsberg, 1984). Using a standard desktop PC (e.g. Intel Q9400 central
296 processing unit CPU @ 2.66 GHz) and a single CPU we observed a forward-modelling speed
297 of about 5-6 points per second. For a total of ~ 18300 $1^\circ \times 1^\circ$ tiles within the SRTM coverage
298 and adjoining marine zones, this translates into a total computation time of about 20 years,
299 underlining the demanding nature of near-global ultra-high resolution forward-modelling and
300 necessitating the use of advanced computational resources and massive parallelization.

301

302 We acknowledge some technique optimizations are possible, e.g., based on efficient tesseroid
303 formulae in place of prisms (Grombein et al., 2013), which however, will not circumvent the
304 need for supercomputing. Alternatively, Fast Fourier Transform (FFT) methods (e.g., Forsberg
305 1985) could be used for a more efficient calculation of gravity effects from RTM data, while
306 the application of FFT for the accurate calculation of RTM vertical deflections is “rather
307 complicated” (Forsberg, 1985, p359). FFT techniques were not deployed in this study.

308

309 To accomplish the forward-modelling we used the Epic supercomputer that is part of Western
310 Australia’s iVEC supercomputing initiative (www.ivec.org) and Pawsey centre, providing
311 advanced resources to Western Australian researchers, particularly in Earth Sciences. Epic is
312 a Linux cluster system that operates a total of 9600 Intel Xeon X5660 CPUs along with 18
313 TB of RAM. With up to 1153 CPUs (or a ~ 12 % share) simultaneously available to us, we
314 completed the gravity forward-modelling task as described before within a period of less
315 than three weeks time, or $\sim 30,000$ CPU-hours. This demonstrates the pivotal role of
316 parallelization and supercomputer deployment for ultra-high resolution forward-modelling at
317 a global scale.

318

319 **2.5 Detection and removal of artefacts**

320

321 Global inspection of the forward-modelling results over our target area showed a number of
322 locations with unrealistically large negative gravity disturbances as small as -1040 mGal. At
323 the locations of these suspicious gravity minima, we identified spike-like depressions in the
324 input topography, both over land areas (SRTM V4.1) and over coastal zones
325 (SRTM30_PLUS V7). We analysed all locations with forward-modelled gravity disturbances
326 smaller than an arbitrary threshold of -400 mGal, and found by visual inspection of the
327 forward-modelled gravity further artefacts present in both elevation data sets. These artefacts
328 are cautiously attributed to

329

- Unfilled holes in the SRTM V4.1 data and interpolation errors along the seams of 1-
330 degree tiles over parts of Asia.

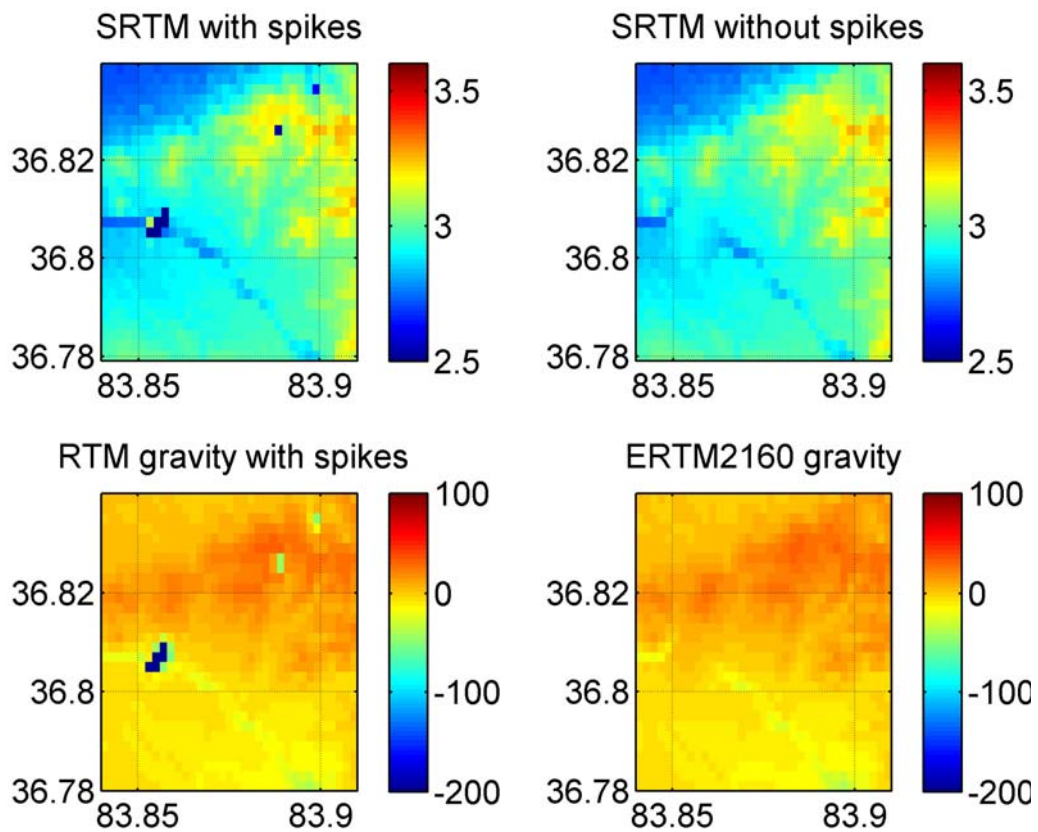
331

- Discrepancies between ship depth-soundings and altimetric depths (SRTM30_PLUS
332 V7) resulting in ‘sea-floor holes’ of up to 5 km.

333 From inspection of all forward-modelled functionals, particularly local minima of gravity
334 disturbances turned out to be very sensitive for unnaturally steep gradients in topography
335 models (which occur at spike-like depressions). In a similar context, this sensitivity was
336 indicated by Kirby and Featherstone (2001, 2002) who detected bad data areas in a national
337 elevation model via gravimetric terrain corrections. We decided to clean the input
338 topography by masking out the affected locations, before filling them with bicubic
339 interpolation. Though this procedure does not recover any information of the terrain shape, it
340 satisfactorily removes the identified artefacts from the input topography. We iteratively
341 repeated all steps of the forward modelling (Sects. 2.1 to 2.4) for computation points within a

342 ~200 km radius around affected areas. From Table 2, the fraction of points with removed
 343 artefacts is 0.001 % for land points and larger for ocean points (0.03 %), suggesting the
 344 overall impact to be comparatively small.

345
 346 We communicated the ‘bad-data’ locations to the producers of SRTM V4.1 and
 347 SRTM30_PLUS V7, confirming the presence of artefacts in their data set. Importantly, these
 348 problems had not necessarily become evident had we restricted the modelling to a regionally
 349 limited area, e.g., European Alps, as done in past research (e.g., Hirt, 2012). Fig. 2 illustrates
 350 the effect of unfilled holes in the SRTM input topography on forward-modelled gravity
 351 disturbances over a moderately affected region, and shows both data sets after hole-filling of
 352 the SRTM data. While we made an attempt to remove notable or striking artefacts from the
 353 input topography through testing against thresholds and visual inspection, less spurious
 354 effects are likely to be present in the forward-modelled gravity (cf. Sect. 5). Complete
 355 cleaning of the input elevation data at 3 billion points remains a challenge, seemingly also for
 356 providers of elevation data sets.
 357



358
 359 **Fig. 2** RTM gravity disturbances before (left) and after spike removal (right). Top: SRTM V4.1
 360 elevations in km, Bottom: short-scale RTM gravity disturbances in mGal.

361
 362
 363

Table 2 Summary of elevation data sets used, and artefacts replaced

Elevation data set	Model resolution (arc-sec)	#ERTM2160 computation points (billion)	#Elevations replaced	Fraction of directly affected ERTM2160 points
SRTM250m V4.1	7.5	~2.9	2913	~0.001%
SRTM30_PLUS	30	~1.7	2977	~0.03 %

364

365

366 3 Results, comparisons and analyses

367

368 3.1 ERTM2160 characteristics

369

370 The main outcome of the gravity forward-modelling procedures described in Sect. 2 is the
 371 ERTM2160 short-scale gravity field model. It provides numerical values for the four
 372 functionals quasi/geoid height, gravity disturbances, North-South and East-West vertical
 373 deflections at 3,062,677,383 locations over the SRTM data area (extended with a ~10 km
 374 buffer over sea) at a spatial resolution of 7.2 arc-sec. The descriptive statistics of ERTM2160
 375 (Table 3) provide for the first time near-global topography-based estimates of Earth’s short-
 376 scale gravity field signal strength (half wavelength of ~10 km down to ~250 m), which are
 377 omitted by degree-2160 spherical harmonic potential models. ERTM2160 can be used to
 378 augment –in approximation– any degree-2160 geopotential model (e.g., EGM2008; Pavlis et
 379 al., 2012) or topographic potential model (e.g., dV_ELL_RET2012, Claessens and Hirt,
 380 2013) beyond harmonic degree 2160, thus reducing the signal omission error (e.g., Gruber,
 381 2009) to some extent. Note that the RTM-technique does not augment the spherical harmonic
 382 model rigorously because the underlying filtering in the topography domain does not exactly
 383 correspond to the filtering in the gravity domain (cf. Section 5).

384

385

386 **Table 3** Descriptive statistics of the ERTM2160 gravity field functionals at 3,062,677,383 land and
 387 near-coastal points between $\pm 60^\circ$ latitude

Functional	Unit	Min	Max	Mean	RMS
Quasi/geoid	m	- 0.280	0.304	0.000	0.016
Gravity disturbance	mGal	-362.4	139.9	-1.050	10.59
North-South vertical deflection	arc-sec	-29.1	31.3	0.000	1.43
East-West vertical deflection	arc-sec	-32.3	29.1	0.000	1.46

388

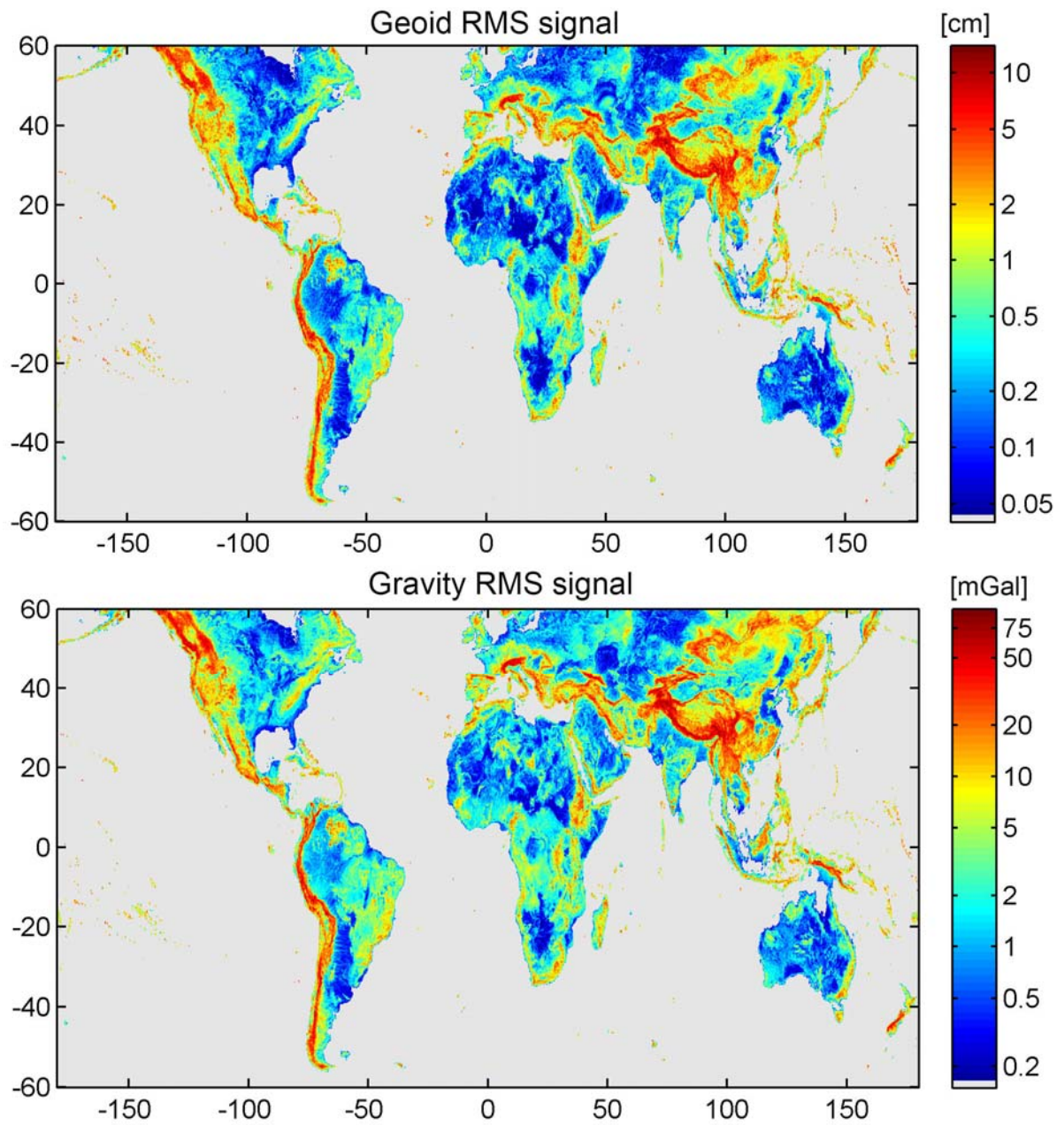
389

390 From Table 3, the ERTM2160 quasi/geoid has a RMS (root-mean-square) signal strength of
 391 1.6 cm (maximum of ~30 cm over the Himalayas), the RMS of gravity disturbances is 10.6
 392 mGal (variation between -360 to +140 mGal), and the RMS signal strength of vertical
 393 deflections is 1.4 arc-sec (maximum ~30 arc-sec). Because of the coverage and point density
 394 reached, we consider these estimates to be robust and globally representative ‘average values’
 395 over land areas of all topography types (flat to high mountains) and adjoining coastal zones.

396

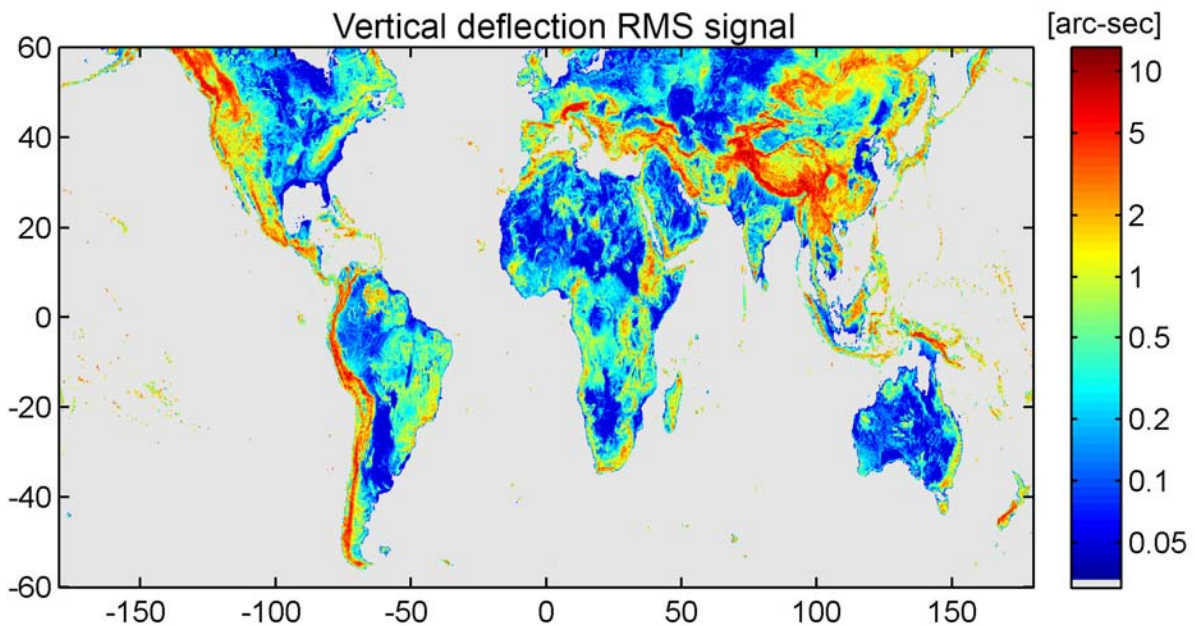
397 Fig. 3 shows the local variability of the RMS signal strengths as computed over $0.1^\circ \times 0.1^\circ$
 398 regions (each covering 10,000 ERTM2160 data points) for geoid effects and gravity
 399 disturbances. The RMS quasi/geoid signals (Fig. 3 top) are mostly below or at the cm-level
 400 over regions with flat topography (i.e., most of Australia), reach 3-4 cm over mountain ranges
 401 such as parts of the Rocky Mountains and Andes, and a maximum RMS strength of ~10 cm
 402 over the Himalaya region. The signal strengths of gravity disturbances (Fig. 3 bottom) and
 403 vertical deflections (shown in Fig. 4) vary qualitatively in a similar way, with maximum
 404 RMS signal strengths of ~70 mGal and ~10 arc-sec present over the Himalayas (Fig. 3
 405 bottom and Fig. 4).

406



407
 408
 409
 410
 411
 412

Fig. 3 Spatially varying ERTM2160 RMS signal strengths. Top: RMS of ERTM2160 quasi/geoid effects in centimeters, Bottom: RMS of ERTM2160 gravity disturbances in mGal



413
414 **Fig. 4** Spatially varying ERTM2160 RMS signal strengths. RMS of ERTM2160 North-South vertical
415 deflection in arc-sec
416

417 3.2 Signal strength as a function of terrain roughness

418
419 As a refinement of the global ERTM2160 statistics, signal strengths for the four gravity
420 functionals were computed as a function of the terrain roughness. A reasonable measure for
421 the local terrain roughness (variability of heights) is the standard deviation (STD) of the RTM
422 elevations calculated within sufficiently small regions. The entire ERTM2160 data area was
423 subdivided into $0.1^\circ \times 0.1^\circ$ tiles, and terrain roughness values were assigned to each tile. Fig.
424 5 shows the spatially varying RMS signal strengths for geoid, gravity and the two vertical
425 deflection components as a function of the terrain roughness (blue dots). There is marked
426 correlation between terrain roughness and gravity signal strengths which varies between
427 0.976 and 0.995 depending on the functional (Table 4).
428

429 It is useful to form classes of different terrain roughness, e.g., variability of heights < 100 m,
430 100 m to 200 m, and so on, and to calculate the gravity statistics within these classes. A
431 generalisation of this idea leads to classes of small class widths (e.g., 20 m) and a subsequent
432 least squares fit of the gravity signal strengths in order to establish the relationship between
433 terrain roughness and gravity signal strengths. The RMS gravity signal strengths were thus
434 calculated over all areas with the same terrain roughness in classes of 20 m width (from 0 to
435 500 m terrain roughness, and larger class width of 100 m from 500 m to 800 m roughness
436 because of the reduced number of data points). The classified RMS signal strengths (red
437 curves in Fig. 5) reveal in fairly good approximation a linear relationship between RMS
438 gravity signal strengths and terrain roughness values. We then fitted the RMS signal strengths
439 (blue points) through least-squares regression lines (without intercept terms/bias fit).
440

441 From a linear regression (green straight lines in Fig. 5), the RMS signal strength per 100 m
442 terrain roughness are ~ 1.7 cm (geoid heights), ~ 11 mGal (gravity disturbances) and ~ 1.5 arc-
443 sec (vertical deflections in North-South and East-West direction), cf. Table 4. These numbers
444 can be used as a “rule of thumb” to easily estimate the magnitude of signals omitted by
445 degree-2160 (or 10 km resolution) potential models for various types of hilly or mountainous
446 terrain anywhere on Earth. For instance, over a rugged terrain with ± 200 m STD, an

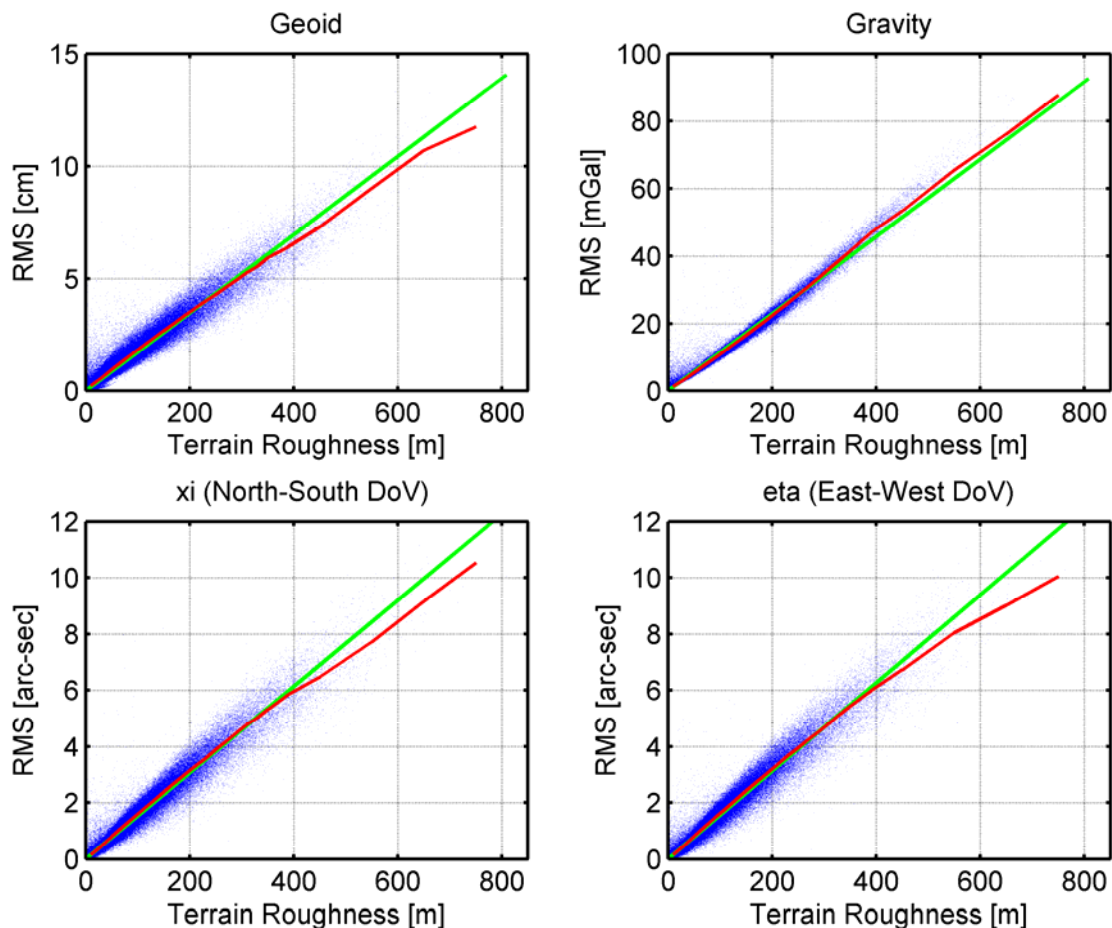
447 omission error of ~ 3.4 cm (geoid height), ~ 22 mGal (gravity disturbances) and ~ 3 arc-sec
 448 (vertical deflections) is to be expected when using the full expansion of the EGM2008
 449 geopotential model. As an aside, the RMS signal strengths per 100 m terrain roughness
 450 (Table 4) are very similar to the (global) RMS signal strengths (Table 3). This is because
 451 globally the mean terrain roughness is 92.6 m which is close to 100 m too.

452

453 **Table 4** Correlation coefficients (between terrain roughness and gravity signal strengths) and gravity
 454 signal strengths per 100 m terrain roughness) for the ERTM2160 gravity field functionals

Functional	Correlation coefficient	RMS signal strength per 100 m terrain roughness
Quasi/geoid	0.976	1.74 cm
Gravity disturbance	0.995	11.5 mGal
North-South vertical deflection	0.981	1.53 arc-sec
East-West vertical deflection	0.982	1.57 arc-sec

455



456

457

458 **Fig. 5** Spatially varying ERTM2160 signal strengths (RMS) as a function of the terrain roughness
 459 (standard deviation of heights) computed over 0.1 degree cells (blue). RMS signal strengths for terrain
 460 roughness classes (20 m class width from 0 to 500 m, 100 m class width beyond) shown in red, and
 461 regression curve (linear model) shown in green. Signal strengths shown for geoid height and gravity
 462 disturbances (top row), and North-South and East-West deflection of the vertical (bottom row).

463

464 **3.3 Comparisons with degree-variance models**

465

466 For comparison purposes, we have compiled estimates for short-scale signal strength from
 467 the literature, which are based on frequently used degree-variance models or modifications
 468 thereof (Table 5). We include estimated RMS signal components from

- 469 (i) the Tscherning-Rapp (1974) model at spatial scales of ~10 to ~1 km, or harmonic
 470 degrees of ~2,000 to 20,000 (numerical values from Torge, 1981; Roland, 2005),
- 471 (ii) the rule of thumb by Kaula (1966), with numerical values from equations provided by
 472 Jekeli et al. (2009), Sanso and Sideris (2013)
- 473 (iii) Jekeli et al. (2009) who fitted a power law model through the EGM2008 power spectral
 474 density between degrees 120 and 1,200, and
- 475 (iv) Sanso and Sideris (2013) who fitted a modified version of the Tscherning-Rapp model
 476 through the EGM2008 signal between degrees 180 and 1,800,
 477 which we compare against those from ERTM2160 (Table 3).

478 RMS signal strengths estimated from the classical Tscherning-Rapp model (that relies on
 479 free-air gravity anomalies) are in good agreement with ERTM2160. For all functionals, the
 480 ERTM2160 signal strengths are somewhat smaller than implied by Tscherning-Rapp (1.6 vs.
 481 2.6 cm, 10.6 vs. 11.8 mGal, and 1.45 vs. 1.75 arc-sec). This could potentially be attributed to
 482 the influence of un-modelled mass-density variations in ERTM2160, but it may also suggest
 483 that the Tscherning-Rapp model slightly overestimates the short-scale signal strength. The
 484 quasi/geoid signal strength estimate from ERTM2160 (1.6 cm) is in between recent estimates
 485 by Jekeli et al. (2009) (4.1 cm) and Sanso and Sideris (2013) (0.5 cm), cautiously suggesting
 486 that the former overestimates and the latter underestimates the quasi/geoid omission error of
 487 degree-2160 geopotential models. Note that ERTM2160 essentially reflects the topography-
 488 implied gravity field characteristics over land, while the power law models are (partially)
 489 based on gravity data over the oceans too, where the gravity field is often smoother.
 490 ERTM2160 signal strengths are found to be mostly smaller than those implied by the power
 491 laws (Table 5). This either indicates underestimation of signal strengths by ERTM2160, or
 492 overestimation through the power laws. Ongoing research attempts to clarify this observation.

493

494 **Table 5** Estimates for short-scale gravity field signals from a cursory literature survey

Model	Functional	Spatial scales	Signal strength	Reference
Tscherning-Rapp	quasi/geoid	~10 to 1 km	2.6 cm	Roland (2005, p7) based on Torge (1981)
	gravity vertical deflection		11.8 mGal 1.75 arc-sec	
Kaula	geoid	< ~10 km	2.9 cm	Jekeli et al. (2009, Eq. 19), Sanso and Sideris (2013, Eq. 3.179)
Power law model based on EGM2008	geoid	<~10 km	4.1 cm	Jekeli et al. (2009, Eq. 23)
Modified Tscherning- Rapp based on EGM2008	geoid	<~10 km	~0.5 cm	Sanso and Sideris (2013, Fig 3.9)

495

496

4 Application examples

The following geodetic applications could benefit from the availability of ERTM2160.

- As a central application, ERTM2160 spectrally enhances degree-2160 geopotential models (e.g., EGM2008) by simple addition of synthesized gravity effects and ERTM2160 gravity. This combination provides spectrally more complete gravity knowledge than provided by degree-2160 models alone, as could be demonstrated by comparisons against ground-truth gravity field observations in several studies (e.g., Hirt, 2010; Hirt et al., 2010; Guimarães et al., 2012; Šprlák et al., 2012; Zhang and Xuebao, 2012; Filmer et al., 2013). This technique can serve a number of applications such as improved GNSS height transfer, in-situ-computation of height system corrections and screening of gravity data bases (Hirt, 2012). ERTM2160 could also be of some utility in the construction of future geopotential models of degree higher than 2160, in analogy to Pavlis et al. (2007; 2012) who used topography to forward model gravity effects at spatial scales of ~10 to ~24 km, and utilized these “fill-in gravity” as additional input for EGM2008.
- For Remove-Compute-Restore (RCR)-based regional gravimetric quasi/geoid computations (e.g., Forsberg and Tscherning, 1981; Tscherning, 2013; Denker, 2013), ERTM2160 gravity disturbances could prove useful as in-situ data source to smooth observed gravity anomalies. Analogously, in astrogeodetic geoid determination based on astronomical-topographic levelling (Hirt and Flury, 2008), ERTM2160 vertical deflections could be used to smooth observed vertical deflection before interpolation.
- Flury (2006) described and applied a range of methods for transforming regional gravity data sets from the space into the frequency domain, and studied the resulting power spectra. While Flury (2006) worked with topographically-reduced gravity anomalies, he pointed out the need to analyse the spectral constituents of topographic gravity signals as well. By applying Flury’s methods on ERTM2160 gravity effects, ‘localised’ or – through averaging – global short-scale power spectra could be obtained, which are useful for further verification or refinement of existing degree-variance models at very short spatial scales.

5 Limitations

For the application of the ERTM2160 topography-implied gravity field model, e.g., as a proxy over regions with scarce gravity data coverage, or as an aid to smooth gravity field observations before interpolation, it is important to be aware of limitations originating from the modelling techniques and topography/bathymetry data used.

First and foremost, the ERTM2160 gravity forward-modelling is based on the assumption of constant mass-density for the residual topography. While the mass-density of major water-bodies (Table 1) has been taken into account as rock-equivalent topography (Sect 2.2), no attempt was made to model local mass-density anomalies as associated with, e.g., salt-domes, valley fillings in the mountains, oceanic sediments. This is mainly because a global digital density data base that would provide 3D information on local mass-density anomalies with sufficient spatial resolution (e.g. Tsoulis, 2013) was not available for this work. ERTM2160 implicitly relies on the assumption of isostatically uncompensated residual topography. Given Earth’s lithosphere thickness often reaches several tens of km (e.g., Watts, 2011), it is reasonable to assume the topographic masses supported at spatial scales less than 10 km.

547 A weakness of the RTM gravity forward-modelling technique, though widely used in
548 practice, is the fact that the spectral characteristics of high-pass filtered elevation data and
549 implied RTM gravity effects are different. In other words, the residual gravity field is not
550 consistent with the residual topography because the relationship between gravity and
551 topography is non-linear (e.g., Rummel et al., 1988). The spectral inconsistency caused by
552 the non-linear relationship can produce additional errors as large as ~6% of the RTM gravity
553 signal (cf. Hirt and Kuhn, 2014, Sect. 4 *ibid*) in case a degree-2160 spherical harmonic
554 topography is used as filter. The investigation of pathways for a correction or reduction (e.g.,
555 filtering in the gravity domain instead of the topography domain, e.g. Baran et al. (2006);
556 Pavlis et al. (2007)) of this issue is a future task.

557
558 While the 7.2 arc-sec spatial resolution of the ERTM2160 short-scale gravity field
559 investigated in our study is much higher than that of any previous global forward-modelling
560 efforts (mostly 1 arc-min in the past), there is still a representation error involved. This is
561 because the very fine structure of the terrain at spatial scales of few metres to ~220 m is not
562 represented by the 7.2 arc-sec topography data used. In rapidly undulating and steep
563 mountainous terrain (e.g., 45° inclination) as an extreme case, the topography representation
564 error associated with 7.2 arc-sec resolution is estimated to reach values as large as ~100 m,
565 which translates into a gravity representation error of ~10 mGal. Use of higher-resolution
566 topography data in future forward modelling efforts will reduce this effect.

567
568 Finally, it is important to note that topography and bathymetry models only ever approximate
569 the geometry of the actual terrain and sea bed only to some extent. While any large-scale (i.e,
570 half-wavelengths of 10 km or more) errors in the elevation data are filtered out in the RTM-
571 approach, short-scale errors will have entered unfiltered in the ERTM2160 gravity field.
572 Although an attempt was made to remove obvious small-scale bad-data areas from the input
573 topography and bathymetry (Sect 2.5), there may be smaller artefacts present in ERTM2160.
574 Particularly along the coastlines of the several hundreds of Pacific islands, the high-pass
575 filtered bathymetry often exhibits peak-like or circular depressions, with an associated ~10-
576 20 mGal gravity effect, in some cases possibly exceeding ~100 mGal. In the absence of
577 independent control (reliable bathymetry or gravimetric observations) over these regions, it is
578 difficult to decide whether these depressions are real or artificial. ERTM2160 may therefore
579 have limitations in coastal zones surrounding islands.

580

581 **6 Concluding remarks**

582

583 The successful development of the ERTM2160 short-scale gravity model demonstrates that
584 ultra-high resolution gravity forward-modelling has become possible at a global scale based
585 on massive parallel computation. As such, ERTM2160 is the first of a new kind of
586 topography-based gravity field representations, which combine localized ultra-high resolution
587 information and near-global coverage. ERTM2160 gravity functionals can be used to
588 augment any degree-2160 harmonic model at spatial scales of ~10 km to ~250 m. This
589 enhances the spatial resolution of EGM2008 or other degree-2160 models by a factor of 40.

590

591 The ERTM2160 model was used to study the characteristics of Earth's short-scale gravity
592 field based on near-global coverage over land areas and ultra-high resolution. Spatially
593 varying statistics were applied to calculate global maps of RTM gravity signal strengths and
594 their dependency on the terrain roughness. The relationship between the RTM gravity signal
595 strengths and terrain roughness values was found to be linear with a correlation of 0.995 for
596 gravity, and slightly lesser correlation for geoid heights and vertical deflections. This was

597 used to establish a new rule of thumb that per 100 m variation in terrain height (standard
598 deviation) gravity field signals of 1.7 cm (geoid), 11 mGal (gravity) and 1.5 arc-sec may be
599 expected at spatial scales of ~10 km to ~250 m. This new rule of thumb may be of value to
600 easily estimate the magnitude of the omission error in gravity signals by degree-2160
601 geopotential models, notably EGM2008 over various types of terrain.

602

603 While a forward-modelling grid-resolution of 7.2 arc-secs – commensurate with the 250 m
604 elevation data – was chosen for this work, a further increase in forward-modelling resolution
605 is likely based on the ever-increasing performance of supercomputing resources. The global
606 calculation of gravity effects at the ~3 arc-sec SRTM basis resolution is foreseeable, as is a
607 further increase to 1 arc-sec (ASTER basis resolution, Tachikawa et al., 2011). The
608 availability of largely clean elevation data – free of artefacts – is crucial in this context.

609

610 **Postscript**

611 Bad data areas, which were detected in the SRTM30_PLUS bathymetry via analysis of
612 ERTM2160 gravity effects and reported to the data producers (Scripps Institution of
613 Oceanography, Prof. Sandwell), have now been rectified in the latest SRTM30_PLUS
614 releases (v9 and v10).

615

616 **Acknowledgements**

617

618 We are grateful to the Australian Research Council (ARC grant DP120102441) and to the
619 Institute of Advanced Study (IAS), TU Munich for funding. We are indebted to iVEC staff
620 for their support and computational resources provided to us. The ERTM2160 model (70 GB)
621 including extraction software will be made publicly available via
622 <http://ddfe.curtin.edu.au/gravitymodels/ERTM2160> and further information will become
623 available via the project website <http://geodesy.curtin.edu.au/research/models/ERTM2160>.
624 Our thanks go to three reviewers for their comments on the manuscript.

625

626 **References**

- 627 Balmino, G., Vales, N., Bonvalot, S., Briais, A., 2012. Spherical harmonic modelling to ultra-high degree of
628 Bouguer and isostatic anomalies. *Journal of Geodesy* 86(7):499-520. doi: 10.1007/s00190-011-0533-4.
- 629 Baran I., Kuhn, M., Claessens, S.J., Featherstone, W.E., Holmes, S.A., Vaníček, P., 2006. A synthetic Earth
630 Gravity Model designed specifically for testing regional gravimetric geoid determination algorithms.
631 *Journal of Geodesy* 80(1):1-16, doi: 10.1007/s00190-005-0002-z.
- 632 Becker, J.J., Sandwell, D.T., Smith, W.H.F., Braud, J., Binder, B., Depner, J., Fabre, D., Factor, J., Ingalls, S.,
633 Kim, S.-H., Ladner, R., Marks, K., Nelson, S., Pharaoh, A., Trimmer, R., Von Rosenberg, J., Wallace,
634 G., Weatherall, P., 2009. Global Bathymetry and Elevation Data at 30 Arc Seconds Resolution:
635 SRTM30_PLUS. *Marine Geodesy* 32(4):355-371, doi: 10.1080/01490410903297766.
- 636 Bonvalot, S., Balmino, G., Briais, A., Kuhn, M., Peyrefitte, A., Vales, N., et al., 2012. World Gravity Map,
637 1:50,000,000 map, Eds.: BGI-CGMW-CNES-IRD, Paris.
- 638 Claessens, S.J., Hirt, C., 2013. Ellipsoidal topographic potential - new solutions for spectral forward gravity
639 modelling of topography with respect to a reference ellipsoid. *Journal of Geophysical Research – Solid*
640 *Earth* 118(11), 5991-6002, doi: 10.1002/2013JB010457.
- 641 Denker, H., 2013. Regional Gravity Field Modeling: Theory and Practical Results. In: G Xu (ed) *Sciences of*
642 *Geodesy - II*, 185-291, Springer, Berlin, Heidelberg. doi:10.1007/978-3-642-28000-9_5.
- 643 Farr, T.G., Rosen, P.A., Caro, E., Crippen, R., Duren, R., Hensley, S., Kobrick, M., Paller, M., Rodriguez, E.,
644 Roth, L., Seal, D., Shaffer, S., Shimada, J., Umland, J., Werner, M., Oskin, M., Burbank, D., Alsdorf, D.,
645 2007. The Shuttle Radar Topography Mission. *Reviews Geophysics* 45:RG2004.
- 646 Filmer, M.S., Hirt, C., Featherstone, W.E., 2013. Error sources and data limitations for the prediction of surface
647 gravity: a case study using benchmarks. *Studia Geophysica Geodetica* 57, 47-66 doi: 10.1007/s11200-
648 012-1114-6.
- 649 Flury, J., 2006. Short wavelength spectral properties of gravity field quantities. *Journal of Geodesy* 79(10
650 11):624-640. doi:10.1007/s00190-005-0011-y.

651 Forsberg, R., Tscherning, C.C., 1981. The use of height data in gravity field approximation by collocation.
652 Journal of Geophysical Research 86(B9), 7843-7854.

653 Forsberg, R., 1984. A study of terrain reductions, density anomalies and geophysical inversion methods in
654 gravity field modelling. Report 355, Department of Geodetic Science and Surveying, Ohio State
655 University, Columbus.

656 Forsberg, R., 1985. Gravity field terrain effect computations by FFT. Bulletin Geodesique 59, 342-360.

657 Grombein, T., Seitz, K., Heck, B., 2013. Optimized formulas for the gravitational field of a tesseroid. Journal of
658 Geodesy 87(7):645–660. doi:10.1007/s00190-013-0636-1.

659 Grombein, T., Luo, X., Seitz, K., Heck, B., 2014. A wavelet-based assessment of topographic-isostatic
660 reductions for GOCE gravity gradients. Surveys in Geophysics, doi: 10.1007/s10712-014-9283-1.

661 Gruber, T., 2009. Evaluation of the EGM2008 Gravity Field by Means of GPS Levelling and Sea Surface
662 Topography Solutions. In: Newton's Bulletin 4:3–17, Publication of the International Association of
663 Geodesy and International Gravity Field Service.

664 Gruber C., Novák P., Flechtner, F., Barthelmes, F., 2013. Derivation of the topographic potential from global
665 DEM models. International Association of Geodesy Symposia 139, Springer-Verlag Berlin, Heidelberg,
666 535-542, doi: 10.1007/978-3-642-37222-3_71.

667 Guimarães, G.N., Matos, A.C.O.C., Blitzkow, D., 2012. An evaluation of recent GOCE geopotential models in
668 Brazil. Journal Geodic Science 2(2):144-155. doi:10.2478/v10156-011-0033-8.

669 Heck, B., Seitz, K., 2007. A comparison of the tesseroid, prism and point-mass approaches for mass reductions
670 in gravity field modelling. Journal of Geodesy 81(2):121-136. doi: 10.1007/s00190-006-0094-0.

671 Hirt, C., Flury, J., 2008. Astronomical-topographic levelling using high-precision astrogeodetic vertical
672 deflections and digital terrain model data. Journal of Geodesy 82(4-5):231-248, doi:10.1007/s00190-007-
673 0173.

674 Hirt, C., Marti, U., Featherstone, W.E., 2010. Combining EGM2008 and SRTM/DTM2006.0 residual terrain
675 model data to improve quasigeoid computations in mountainous areas devoid of gravity data. Journal of
676 Geodesy 84(9):557-567. doi:10.1007/s00190-010-0395-1.

677 Hirt, C., 2010. Prediction of vertical deflections from high-degree spherical harmonic synthesis and residual
678 terrain model data. Journal of Geodesy 84(3): 179-190. doi:10.1007/s00190-009-0354-x.

679 Hirt, C., 2012. Efficient and accurate high-degree spherical harmonic synthesis of gravity field functionals at the
680 Earth's surface using the gradient approach. Journal of Geodesy 86(9):729-744. doi:10.1007/s00190-012-
681 0550-y.

682 Hirt C., Fecher, T., Claessens, S.J., Kuhn, M., Pail, R., Rexer, M., 2013. New ultra-high resolution picture of
683 Earth's gravity field. Geophysical Research Letters, 40(16), 4279-4283, doi: 10.1002/grl.50838.

684 Hirt, C., 2013. RTM gravity forward-modeling using topography/bathymetry data to improve high-degree
685 global geopotential models in the coastal zone. Marine Geodesy 36(2):1–20.
686 doi:10.1080/01490419.2013.779334.

687 Hirt, C., Kuhn, M. 2014. A band-limited topographic mass distribution generates a full-spectrum gravity field –
688 gravity forward modelling in the spectral and spatial domain revisited. Journal of Geophysical Research
689 – Solid Earth 119, doi:10.1002/2013JB010900.

690 Jacoby, W., Smilde, P.L., 2009. Gravity interpretation, Springer, Berlin, Heidelberg.

691 Jarvis, A., Reuter, H.I., Nelson, A., Guevara, E., 2008. Hole-filled SRTM for the globe Version 4. Available
692 from the CGIAR-SXI SRTM 90m database: <http://srtm.csi.cgiar.org>.

693 Jekeli, C., Yanh, H.J., Kwon, J.H., 2009. Evaluation of EGM08 - globally and locally in South Korea. In:
694 Newton's Bulletin 4:39-49, Publication of the International Association of Geodesy and International
695 Gravity Field Service.

696 Kaula, W., 1966. Theory of satellite geodesy, Blaisdell Pub. Co.

697 Kirby, J.F., Featherstone, W.E., 2001. Anomalous large gradients in the “GEODATA 9 Second” digital
698 elevation model of Australia, and their effects on gravimetric terrain corrections. Cartography 30:1–10.

699 Kirby, J.F., Featherstone, W.E. 2002. High-resolution grids of gravimetric terrain correction and complete
700 Bouguer corrections over Australia. Exploration Geophysics 33(4):161–165. doi:10.1071/EG00109.

701 Kuhn, M., Seitz, K., 2005. Comparison of Newton's integral in the space and frequency domains. In: Sansò F
702 (ed) A window on the future of geodesy. IAG symposia 128:386-391, Springer, Berlin, Heidelberg,
703 doi:10.1007/3-540-27432-4_66.

704 Kuhn, M., Featherstone, W.E., Kirby, J.F., 2009. Complete spherical Bouguer gravity anomalies over Australia.
705 Austral J Earth Sci 56(2):213-223. doi:10.1080/08120090802547041.

706 Nagy, D., Papp, G., Benedek, J., 2000. The Gravitational Potential and its Derivatives for the Prism. J. Geod
707 74(7-8):552-560. doi:10.1007/s001900000116, Erratum in J Geod 76(8):475. doi:10.1007/s00190-002-
708 0264-7.

709 Pavlis, N.K., Factor, J.K., Holmes, S.A., 2007. Terrain-related gravimetric quantities computed for the next
710 EGM. Proceedings of the 1st International Symposium of the International Gravity Field Service (IGFS),
711 Istanbul, 318-323.

712 Pavlis, N.K., Holmes, S.A., Kenyon, S.C., Factor, J.K., 2012. The development and evaluation of the Earth
713 Gravitational Model 2008 (EGM2008). *Journal Geophysical Research* 117, B04406.
714 doi:10.1029/2011JB008916. Correction in *Journal Geophysical Research* 118, 1–1,
715 doi:10.1002/jgrb.50167.

716 Reuter, H.I., Nelson, A., Jarvis, A., 2007. An evaluation of void filling interpolation methods for SRTM data.
717 *International Journal Geographic Information Science* 21(9): 983–1008.

718 Roland, M., 2005. Untersuchungen zur Kombination terrestrischer Schweredaten und aktueller globaler
719 Schwerefeldmodelle. *Wissenschaftliche Arbeiten der Fachrichtung Geodäsie und Geoinformatik an der*
720 *Universität Hannover* Nr. 255.

721 Rummel, R., Rapp, R.H., Sünkel, H., Tscherning, C.C., 1988. Comparisons of global topographic/isostatic
722 models to the Earth's observed gravity field. Report No 388, Dep. Geodetic Sci. Surv., Ohio State
723 University, Columbus, Ohio.

724 Sansò, F., Sideris, M., 2013. Harmonic Calculus and Global Gravity Models. In: F. Sansò and M.G. Sideris
725 (eds) *Geoid Determination, Lecture Notes in Earth System Sciences* 110:111-168, Springer, Berlin,
726 Heidelberg. doi:10.1007/978-3-540-74700-0_3.

727 Šprlák, M., Gerlach, C., Pettersen, B.R., 2012. Validation of GOCE global gravity field models using terrestrial
728 gravity data in Norway. *Journal Geodetic Science* 2(2):134-143.

729 Tachikawa, T., et al., 2011. ASTER Global Digital Elevation Model Version 2 – Summary of Validation
730 Results, [https://www.jspacesystems.or.jp/ersdac/GDEM/ver2Validation/Summary_GDEM2_validation_r](https://www.jspacesystems.or.jp/ersdac/GDEM/ver2Validation/Summary_GDEM2_validation_report_final.pdf)
731 [eport_final.pdf](https://www.jspacesystems.or.jp/ersdac/GDEM/ver2Validation/Summary_GDEM2_validation_report_final.pdf).

732 Torge, W., 1981. *Resultate und Probleme der Geoidbestimmung*. *Wissenschaftliche Arbeiten der Fachrichtung*
733 *Vermessungswesen der Univ. Hannover* Nr. 100.

734 Tscherning, C.C., Rapp, R., 1974. Closed covariance expressions for gravity anomalies, geoid undulations and
735 deflections of the vertical implied by anomaly degree variance models. Report No 355, Dep. Geodetic
736 Sci. Surv., Ohio State University, Columbus, Ohio.

737 Tscherning, C.C., 2013. Geoid Determination by 3D Least-Squares Collocation. In: F Sanso and MG Sideris
738 (eds) *Geoid Determination, Lecture Notes in Earth System Sciences* 110:311-336, Springer, Berlin,
739 Heidelberg. doi:10.1007/978-3-540-74700-0_7.

740 Tsoulis, D., 2013. Geodetic use of global digital terrain and crustal databases in gravity field modeling and
741 interpretation. *Journal Geodetic Science* 1(Mar 2013):1-6.

742 Tziavos, I.N., Sideris, M.G., 2013. Topographic Reductions in Gravity and Geoid Modeling. In: F Sanso and
743 MG Sideris (eds), *Geoid Determination, Lecture Notes in Earth System Sciences* 110:337-400, Springer,
744 Berlin Heidelberg. doi:10.1007/978-3-540-74700-0_8.

745 USGS, 1996. USGS (U.S. Geological Survey) Global 30-Arc-Second Elevation Data Set. U.S. Geological
746 Survey, Sioux Falls, South Dakota. http://webgis.wr.usgs.gov/globalgis/gtopo30/gtopo_ab.htm.

747 Watts, A.B., 2011. Isostasy. In: *Encyclopedia of Solid Earth Geophysics* (Ed. Gupta, H. K.), 984 1, 647-662,
748 Elsevier.

749 Zhang, X., Xuebao, L.C., 2012. The approach of GPS height transformation based on EGM2008 and
750 SRTM/DTM2006.0 residual terrain model. *Acta Geod Cart Sin* 41(1):25-32.

751